

Space Shuttle Boundary Layer Transition Flight Experiment Ground Testing Overview

Karen T. Berger¹

NASA Langley Research Center, Hampton, VA

Brian P. Anderson² and Charles H. Campbell³

NASA Johnson Space Center, Houston, TX

Abstract

In support of the Boundary Layer Transition (BLT) Flight Experiment (FE) Project in which a manufactured protuberance tile was installed on the port wing of Space Shuttle Orbiter Discovery for STS-119, STS-128, STS-131 and STS-133 as well as Space Shuttle Orbiter Endeavour for STS-134, a significant ground test campaign was completed. The primary goals of the test campaign were to provide ground test data to support the planning and safety certification efforts required to fly the flight experiment as well as validation for the collected flight data. These test included Arcjet testing of the tile protuberance, aerothermal testing to determine the boundary layer transition behavior and resultant surface heating and planar laser induced fluorescence (PLIF) testing in order to gain a better understanding of the flow field characteristics associated with the flight experiment. This paper provides an overview of the BLT FE Project ground testing. High-level overviews of the facilities, models, test techniques and data are presented, along with a summary of the insights gained from each test.

Symbols

M_e	Mach number at the edge of the boundary layer
Re_θ	Reynolds number based on momentum thickness
δ	Boundary Layer Thickness (in)

Introduction

The design and ultimate weight of any vehicle entering a planetary atmosphere is affected by the amount of thermal protection system (TPS) required for safe and successful entry. One of the design drivers to TPS sizing is the time during the entry at which the boundary layer transitions from laminar to turbulent flow. The study of BLT has been a significant effort for many decades, but the specific physics-based mechanisms that cause hypersonic BLT are poorly understood. This lack of understanding hinders designers in making accurate predictions of when the boundary layer will become turbulent and affects the sizing or the understanding of TPS robustness. If the geometry of a vehicle is known, engineers can obtain ground-test data from wind tunnels to develop engineering correlations.¹⁻⁴ However, one of the major weaknesses in a ground-based correlation approach is lack of understanding of the differences between wind tunnel and flight environments and how those differences affect BLT.

In support of the Space Shuttle BLT Flight Experiment,^{5, 6} a ground testing program was initiated, including entries in the facilities at the National Aeronautics and Space Administration (NASA) Johnson Space Center (JSC) and NASA Langley Research Center (LaRC) as well as Calspan-University of Buffalo Research Center (CUBRC). The JSC arc jet testing was critical for the initial analysis, safety certification and the flight rationale for the flight experiment. A later entry was used to provide confidence in the thermal predictions/certifications as well as an understanding of the material failure behavior and survivability of the TPS material for larger protuberance heights. Testing in the other wind tunnels provided data on the effectiveness of various boundary layer trip configurations and heights (though all but one of the wind tunnel tests were run after the first flight of the flight experiment) as well provided data for future improvements to ground-to-flight extrapolation techniques. The ground test data complimented a larger set of aeroheating data including computational predictions, both discrete and global ground test

¹ BLT Flight Experiment Principal Investigator, Aerothermodynamics Branch, M/S 408A

² Aerospace Engineer, Applied Aeroscience and CFD Branch, M/C EG3

³ Deputy BLT Flight Experiment Principal Investigator, Applied Aeroscience and CFD Branch, M/C EG3

data as well as discrete and global flight data. While some of the tests were completed in direct support of the flight experiment program, others were completed in support of the Hypersonic Thermodynamic Infrared Measurements (HYTHIRM) Team⁷ and the Fundamental Aeronautics Program (FAP) but used the flight experiment protuberance configurations and/or location and are covered in this report. This report will document the flight experiment (briefly), the facilities, test techniques, models and data from all of the Space Shuttle BLT FE related ground tests.

Boundary Layer Transition Flight Experiment

BLT occurred on all Space Shuttle re-entries, nominally between Mach 8 and Mach 5.5, and usually as a result of the inherent roughness on the vehicle (steps and gaps in the tile TPS), but could occur earlier when damage or protruding gap fillers were present. Historically, the earliest this was recorded was Mach 17.6 on STS-28 and Mach 19.4-17.3 on STS-73 (both on Orbital Vehicle (OV)-102, *Columbia*). Following the STS-107 loss of *Columbia*, the Orbiter Damage Assessment Team (DAT) was established with a charter to assess the effects of ascent and on-orbit damage and impacts upon the ability to perform safe re-entry.⁸ A substantial ground testing and analytical tool development activity was undertaken to characterize the aeroheating, thermal and stress implications of damage on the Orbiter material temperatures, tile factors of safety, and structural margins. Aeroheating tools developed included the BLT Tool^{3, 8-10} and the Cavity Heating Tool.^{8, 11} Uncertainties associated with the BLT Tool and the analysis of protruding gap fillers found during STS-114 inspections led to an unprecedented repair spacewalk to remove the gap fillers.¹² As a result of this, a flight test using a protuberance on the Orbiter to purposefully trip the boundary layer at a prescribed Mach number was proposed and approved.¹³

The flight experiment protuberance was placed on the port wing of the vehicle, outboard and downstream of the main landing gear door (Figure 1). This area had available instrumentation wiring as well as was less prone to experience launch related damage. Summary information on the protuberance heights and targeted BLT onset Mach numbers can be found in Table 1. The height of the protuberance was derived using the Orbiter BLT Tool⁹, Version 2 with a Re_{θ}/M_e versus $(k/\delta)(H_w/H_s)$ methodology using a best estimate correlation coefficient established from historical Orbiter flight data. The length and width of the protuberance installed on the vehicle were 4.0-in and approximately 0.4-in, respectively, for all flights. The protuberance leading edge was oriented at an angle of $45 \pm 3^\circ$ relative to the predicted local flow streamline.

Table 1: Summary of BLT FE Flights

Flight	Protuberance Height (in)	Target BLT Onset (Mach Number)	Vehicle	Landing Date
STS-119	0.25	15	<i>Discovery</i> (OV-103)	March 28, 2009
STS-128	0.35	18	<i>Discovery</i> (OV-103)	September 11, 2009
STS-131	0.35	18	<i>Discovery</i> (OV-103)	April 20, 2010
STS-133	0.50	19.5	<i>Discovery</i> (OV-103)	March 9, 2011
STS-134	0.50	19.5	<i>Endeavour</i> (OV-105)	June 1, 2011

Additional instrumentation was added to both *Discovery* and *Endeavour* because prior to the flight experiment, none of the windward thermocouples on either vehicle were located in the expected turbulent wedge. Figure 2 shows a sketch of the location of the instrumentation for *Discovery*. Additional information about the instrumentation can be found in Reference 14.

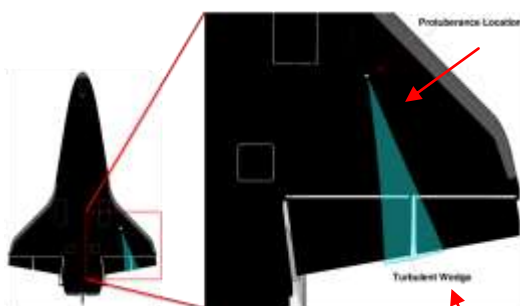


Figure 1: Protuberance location

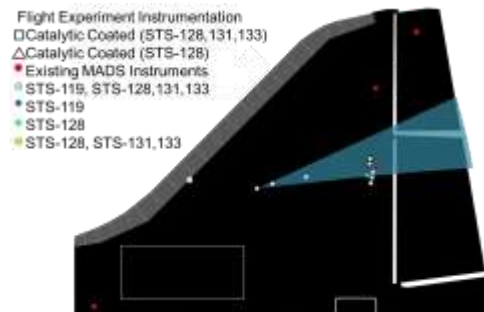


Figure 2: Instrumentation locations

Ground Test Facilities

NASA Johnson Space Center Arc Jet Test Facility

The JSC arc-jet test facility, known as the Atmospheric Reentry Materials and Structures Facility (ARMSEF), is described in detail in Reference 15 and shown in Figure 3. Test position one (TP1) is the channel nozzle arc-jet used to study flat surface heat transfer at zero degree angle of attack. The facility has a 10 MW arc heater and a 12-ft dia. test vacuum chamber with a diffuser. A solid-state power supply, water cooling system, boiler, 4-stage steam ejector system, vacuum pumping system, test gas supply system, control room, and data room are common and can serve either TP 1 or the other test position. The arc heater contains a multi-pack dual-diameter constricted arc column. A tungsten cathode is used as the upstream electrode, and a conical copper anode is used as the downstream electrode. The arc heater contains a variable number of individually water-cooled and electrically insulated constrictor segments assembled in modular packs, 18-20 segments each. The number of packs in the arc heater varies from 5 to 14 to achieve various levels of gas bulk enthalpy with this test program using 10 and 14 packs. The vacuum chamber corresponds to approximately 204,000-182,000 ft altitude. TP1 is configured with a 2-in wide rectangular channel nozzle expanding from a 2x2-in throat at a 10° half angle and can accommodate flat plate specimens as large as 24x24 in. A test section schematic is shown in Figure 4.



Figure 3: NASA JSC Arc Jet Test Facility

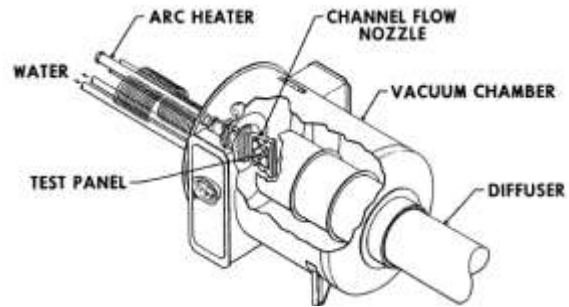


Figure 4: Schematic of Arc Jet Test Section

CUBRC LENS I Tunnel

Aerothermal tests were performed in the CUBRC Large Energy National Shock (LENS)-I Tunnel, a hypervelocity reflected shock tunnel. More detailed information about the facilities can be found in reference 16 and an image of the facility is shown in Figure 5. LENS I has the capability to duplicate flight conditions at Mach numbers ranging from 6 to 15. A diagram of the basic operations of the LENS facilities is shown in Figure 6. The facility includes a 25.5-foot long, 11-inch diameter electrically heated driver tube, a double diaphragm assembly, a 60-foot by 8-inch diameter driven tube, a fast acting centerbody valve assembly, multiple nozzles to achieve desired test conditions and a test section capable of accommodating models up to 3 feet in diameter and 12 feet long. The high-pressure driver section can operate at 30,000 lb_f/in² using heated driver gases of hydrogen, helium, nitrogen or any combination of the three. The driver gases can be heated up to 750°F and the amount of each gas varied to achieve interface operations for maximum test times. The driven tube can use air, nitrogen, carbon dioxide, helium, hydrogen or combinations of gases for model testing.



Figure 5: LENS Hypersonic Shock Tunnel

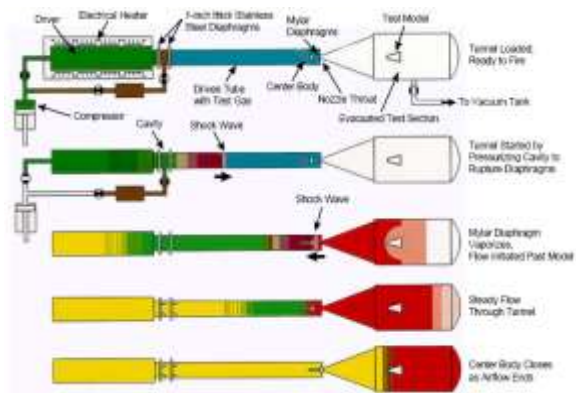


Figure 6: Basic Operations of LENS Facilities

as the test gas. Typical operating conditions for the tunnel were stagnation pressures ranging from 60 to 2000 psia, stagnation temperatures up to 1300 deg R, freestream unit Reynolds numbers from 0.01 to 0.55 million per ft., freestream gamma of 1.21, post normal shock gamma of 1.1, and a normal shock density ratio of 11.7. A contoured axisymmetric nozzle was used to provide a nominal freestream Mach numbers from 5.9 to 6.0. The nozzle exit diameter was 20 in with the flow exhausting into an open jet test section; the nozzle throat diameter was 0.466 in. The test core varied from 12 to 14 inches depending on the operating condition. A floor-mounted model injection system could inject models from a sheltered position to the tunnel centerline in less than 0.5 s. For heat-transfer and flow visualization tests, the model residence time in the flow was only a few seconds; nominal run time for force & moment testing was approximately 20 s.

Test Techniques

Global Phosphor Thermography (LaRC)

The two-color relative-intensity phosphor thermography measurement technique was used to obtain global experimental aeroheating data on models.¹⁸⁻²⁰ This technique uses a mixture of phosphors that fluoresce in the bands of the visible spectrum when illuminated with ultraviolet light. The red and green bands are utilized and the intensity of the fluorescence is dependent upon the amount of incident ultraviolet light and the local surface temperature of the phosphor. This phosphor mixture, which is suspended in a silica ceramic binder and applied with an air brush, is used to coat slip cast silica ceramic models. The final coating thickness is approximately 0.001 in. Using a 3-CCD (Charge Coupled Device) camera, fluorescence intensity images of an illuminated phosphor model exposed to the heated hypersonic flow of the tunnel are acquired and converted to temperature mappings via a temperature-intensity calibration. The temperature-intensity calibration uses the ratio of the red and green components of the image to construct a lookup table which converts the intensities to temperature values. The calibration is valid over a temperature range from 532 °R to 800 °R. The temperature data from the time-sequenced images taken during the wind tunnel run are then reduced to enthalpy based heat transfer coefficient at every pixel on the image (and hence globally on the model) using a heat-transfer calculation assuming one-dimensional semi-infinite slab heat conduction and a step function in the heat transfer coefficient, h .¹⁹ An illustration of the test technique is shown in Figure 10.



Figure 9: LaRC 20-In Mach 6 CF₄ Tunnel

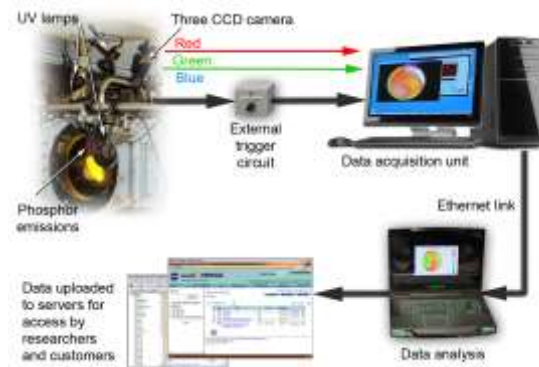


Figure 10: Global Phosphor Thermography

Planar Laser Induced Fluorescence (LaRC)

The PLIF system consists of the laser system, beam-forming optics and a dual-camera detection system. Detailed information about the laser system can be found in Reference 16. The laser system operates at 10 Hz, with about 10 ns pulse duration and tuned to a wavelength of 226.256 nm. The laser beam is directed to the tunnel, as shown in Figure 11, using a series of prisms. Lenses then form the laser beam into a sheet. The sheet is approximately 0.0079 in thick and diverges slightly to a width of about 6 in to illuminate the flow of Nitric Oxide (NO) gas above the surface of the model. Images are acquired using a pair of Princeton Instruments PI-MAX II intensified CCD cameras with 512x512 pixel resolution. One camera uses a Nikon 105-mm focal length, F/4.5 ultraviolet (UV) Nikkor lens. The other uses a Cerco 45-mm focal length, F/1.8 UV lens, resulting in approximately 3 times larger field of view. The spatial resolutions are 249 pix/in. and 81 pix/in. for the two cameras, respectively. The laser sheet

can be translated in the tunnel, allowing measurements at different locations in the flow, both along and away from a surface.

A custom built MHz-rate PLIF imaging system was also used for the testing. The system has a maximum frame rate of 1 MHz and a total available resolution of 160 x 160 pixels. The download time between image sequences is greater than 4 seconds, resulting in a 0.2 Hz repetition rate for the MHz laser/camera system to acquire bursts of pulses.

An additional capability under development for use in the LaRC 31-Inch Mach 10 Air Tunnel is molecular tagging velocimetry (MTV) using the same PLIF camera and laser systems. A 50-mm LaserOptik GmbH diffusion welded lens array of 25, 1-m focal length cylindrical lenses is used to focus the laser sheet into 25 lines to allow for tagging of multiple lines of NO in a single run. A Cooke DiCAM-PRO camera, with a 1280x1024 pixel array interline progressive scan CCD is used. Spatial resolution varies from 398.8 pixels/inch to 444.5 pixels/inch. In double shutter mode, the camera acquires an image pair with a minimum 500 ns delay between the end of the first gate and the beginning of the second. Additional information on the MTV test technique can be found in references 21 and 22.



Figure 11: LaRC Planar Laser Induced Fluorescence

Thermal Measurements (Thin Films – CUBRC)

The large heating rates in the LENS facility mandate the use of rugged aerothermal instrumentation capable of operating for test durations of up to 100 msec. Platinum thin-film heat transfer gages (Figure 12) employed for this test have proven to be the most accurate measurement technique in the LENS I test facilities. The small size of the sensing element along with the insulating substrate make them ideal for measuring surface heating at a high resolution level.^{16, 23, 24} The theory of heat conduction is used to relate the surface temperature history to the rate of heat transfer. Since the platinum resistance element has negligible heat capacity, and hence negligible effect on the Pyrex surface temperature, the gage can be characterized as being homogeneous and isotropic with properties corresponding to those of the Pyrex. Furthermore, because of the short duration of shock tunnel tests, the Pyrex can be treated as a semi-infinite body. CUBRC has calculated the accuracy of the heat transfer measurement to be $\pm 5\%$.



Figure 12: CUBRC Thin Film Heat Transfer Instrumentation (0.125-inch and 0.050-inch diameters)

Schlieren (LaRC)

The NASA LaRC Hypersonic Tunnels are all equipped with pulsed white-light, Z-pattern, single-pass Schlieren systems with a field of view encompassing part or all of the test section. Images are recorded on a high resolution digital camera and/or video camera.

Thermal Measurements (Thermocouples – Arcjet)

The JSC arc jet facility model was equipped with surface, sidewall and bondline thermocouples. Type R thermocouples, capable of reading temperatures as high as 3200 deg F, were used for the surface and sidewall measurements. Type K thermocouples, capable of reading temperatures up to 2490 deg F were used for the bondline measurements. The total temperature measurement uncertainty in these tests did not exceed $\pm 2\%$ (including the data acquisition system) of the measured value for both surface and bondline thermocouples.²⁵ X-ray images of each protuberance tile insert were taken pre-test in order to check the surface thermocouple proximity to the tile outer mold line (OML).

Temperature Sensitive Paints (LaRC, CUBRC, Arc Jet)

The temperature sensitive paint (TSP) system employed in the NASA LaRC 31-Inch Mach 10 study is formulated by dissolving luminophore ruthenium trisbipyridine (RUBY) in a commercially available clear urethane sealant and then applying it to the model using conventional spraying techniques.²⁶ A white acrylic primer is applied to the surface to act as a basecoat to enhance adhesion of the urethane sealant as well as enhance scattering of the luminescence intensity back to the camera. Calibration of the TSP is performed in a laboratory calibration chamber. The TSP formulation displays adequate sensitivity up to about 296 deg F. TSP data in the wind tunnel facility is acquired by illuminating the surface with several light emitting diodes (LED) based arrays with wavelengths of 400 nm. Images are collected using a 14-bit thermoelectrically cooled digital camera with an array size of 2048 x 2048 pixels. TSP images are acquired every 500 ms throughout the run, with the model spending approximately 5-7 sec on centerline. TSP heating maps are normalized to the Fay-Riddell stagnation point heating value.

The TSP coatings employed at CUBRC consists of an insulator, binder and luminophore Ruthenium(phen). The process used is similar to that employed by NASA LaRC and more information can be found in reference 27.

In the arc jet testing at JSC, Tempilaq® temperature-indicating paint was applied to the tiles in locations that were unlikely to see flow disturbances associated with the protuberance heating. Six different grades of paint that melt at various set temperatures, 1500, 1600, 1700, 1800, 1900 and 2000 deg F, were used. The intent of using the paint was to obtain an additional indication of the smooth tile surface temperature, as well as determine the usefulness of such paint for a possible application in the flight experiment. More detailed information about the paint can be found in reference 28.

Wind Tunnel Models

Arc Jet Models (JSC)

Testing in the NASA JSC ARMSEF involved 0.25-inch and 0.35-inch flight protuberances. The test articles were fabricated as part of a 6x6-inch tile made of Boeing Replacement Insulation (BRI)-18 material and coated with reaction cured glass (RCG), similar to the flight tile preparation. The full test article (Figure 13) was a 2x2-foot variable configuration tile array (VCTA) with a cavity designed for the protuberance tile inserts, allowing rapid replacement of the protuberance tiles. The remaining tiles in the VCTA were initially Lockheed Insulation (LI)-900 however later entries replaced three of them with LI-2200 tiles. All tiles were 2-inches thick. The protuberance tiles were installed with the protuberance forward surface at 45-degrees to the local stream line. There were five surface and six bondline thermocouples in the array as well as four surface thermocouples on the protuberance itself. The test articles were X-rayed prior to testing to determine the exact location of the thermocouples in the tile. Tempilaq® temperature-indicating paint locations are evident in the figure, with six dabs of paint in each of the two locations. More detailed information about the wind tunnel model can be found in reference 28. The test articles were scanned prior to and after testing with the Advanced Topical Optical Scan (ATOS) system in order to help document any surface/geometry changes that might occur during testing.

MH-13 Model (CUBRC)

During the Space Shuttle Return-to-Flight Program a 1.8% scale steel and aluminum model, denoted MH-13 (Figure 14), was designed, constructed and instrumented at CUBRC. The model was designed to incorporate a large amount of instrumentation, accept various cavity and trip blocks and rings and have movable control surfaces. Initially the model had ~100 sensors on the centerline and wings and ~200 sensors in the wind leading edge. The starboard wing was instrumented with TSP. Prior to the BLT FE testing eighteen thin-film sensors were added in locations similar to those on the STS-119, -128, -131 and -133 BLT FE flights. Protuberances were fabricated/instrumented to approximately represent the flight

protuberance on the both wings (to maximize data). A diagram of the locations of the new instruments can be found in Figure 15. Additional information about the model can be found in Reference 24.



Figure 13: Tile Test Array and Instrumentation Layout



Figure 14: MH-13 Model in LENS-I

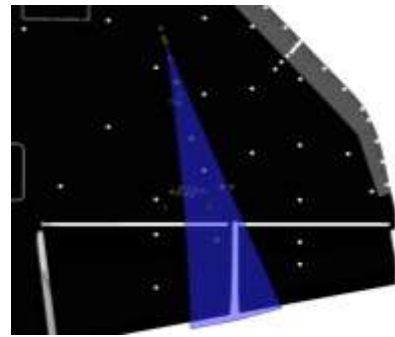


Figure 15: MH-13 Model: BLT FE instrumentation

Ceramic Models (LaRC Mach 6 Air, Mach 6 CF4 and Mach 10 Air)

For the phosphor thermography testing in the NASA LaRC facilities, two different sets of ceramic wind tunnel models were utilized. One set of tests used 0.75% scale ceramic models with 0.05x0.05-in kapton tape boundary layer trips of varying thicknesses (trips did not represent the scaled dimensions of the flight protuberance). A subset of the 0.75% scale models were fabricated with deflected control surfaces (body flap and elevons) to simulate the flight vehicle configuration during the STS-119 and -128. The individual control surface deflections can be found in Table 2. One of the models, installed in the 20-Inch Mach 6 Air Tunnel, is shown in Figure 16. The other set of tests utilized 0.9% scale models of the orbiter with undeflected control surfaces and fence boundary layer trips that were machined into metal rods and installed into the wings of the models (fabricated to represent the scaled flight protuberances). A drawing of the windward surface of the wind tunnel model is shown in Figure 17 and two trips were installed on each model (port and starboard wings) in order to maximize the data collected during the tests. The final trips used were fabricated by EDM Dept., Inc. (Figure 18) and included trips B (0.006-in), C (0.010-in), D (0.015-in), E (0.0175-in) and F (0.020-in). The models tested were B-D and C-E in the Mach 6 Air Tunnel and D-F in the Mach 10 Tunnel. An earlier set was fabricated at NASA LaRC²⁹ but was less geometrically consistent and resulted in trip heights that varied across the protuberance and did not match original specifications. As a result, any data from those trips was identified by the average measured protuberance height and not the design height. Standard methods, materials and equipment developed at LaRC were used in fabricating the ceramic aeroheating test models³⁰. All models had 0.75-in. cylindrical stings.



Figure 16: 0.75% Scale Ceramic Model

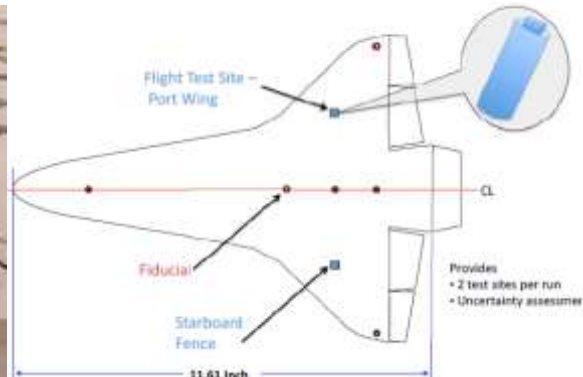


Figure 17: 0.9% Scale Ceramic Model

Table 2: As Flown Control Surface Deflections for STS-119 and 128

Shuttle Mission	Mach Number	Body Flap (deg)	Port Inboard Elevon (deg)	Port Outboard Elevon (deg)	Starboard Inboard Elevon (deg)	Starboard Outboard Elevon (deg)
STS-119	8.43	1.851	-4.484	-4.256	-7.616	-7.558
STS-128	14.73	7.544	-0.946	-0.781	-2.048	-1.998

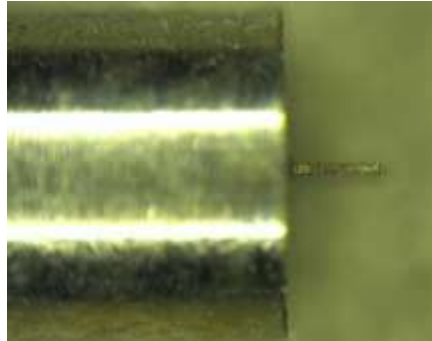


Figure 18: Profile Images EDM Dept. Inc. Protuberances

PLIF and TSP Models (LaRC Mach 10)

The test article for PLIF and TSP testing²⁶ was a 20° full-angle wedge with a sharp leading edge, oriented at 20° to the flow and shown as a computer rendering in Figure 19. The top surface of the wedge was a flat plate, 5 in. wide and 6.4 in. long. Two different protuberance shapes were utilized. One was modeled after the BLT DTO flight experiment protuberance, but scaled to be 0.039-in. or 0.098-in. tall, with a width of approximately 0.42 in and oriented to 45° with respect to the flow. The stereolithography (SLA) material used to make the protuberance was a high-temperature nanocomposite material (NanoForm™ 15120 from DSM Somos), primed and painted with temperature sensitive paint. A rectangular fence trip was also utilized, oriented at the same 45° angle, with a height of 0.039 in., painted black and with sharp edges and corners. NO gas was seeded flow through a spanwise-oriented slot on the model centerline. Flow rates were 150 or 300 standard cubic centimeters per minute (scm).

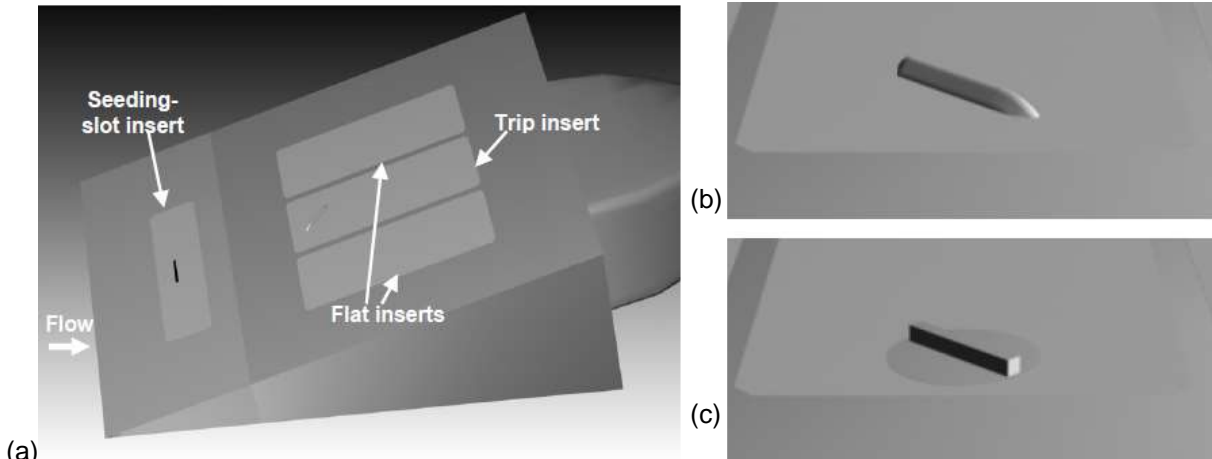


Figure 19: PLIF/TSP Model: (a) Full model, (b) BLT protuberance, (c) rectangular protuberance

Ground Testing Summaries

A significant ground testing campaign was undertaken both prior to and during the flight testing phase of the program. The following sections outline the information collected in each of the tests. Table 3 includes information for each entry including the facility, test dates, number of runs, test conditions and purpose of the testing.

Table 3: Ground Test Summary

Test #	Facility	Date	# of Runs	Mach #	AoA (deg)	Re # (x10 ⁶ /ft)	Beta (deg)	Trip (in)	Test Techniques	Purpose
	ARMSEF	6/08, 10/09-12/09	7		0			0.25, 0.35	TC, TSP	Determine failure modes/survivability
6949	LaRC M6 Air	4/08-5/08	49	6	30- 40	1.1 – 4.1	0,2,4	0-0.0115	GPT, S	Heating associated with the protuberance
	CUBRC	Spring 2010	10	14	40	0.2 – 2.1	0	0.0075, 0.015	TF, TSP	Discrete data with scaled flight trip
170	LaRC M6 CF ₄	9/10	12	6	37.7, 42	0.1 – 3.3	0	0-0.015	GPT, S	Global data to match the HYTHIRM
475	LaRC M10 Air	9/10	16	10	37.7, 42	0.5 – 2.0	0	0-0.015	GPT, S	Global data to match the HYTHIRM
6963	LaRC M6 Air	8/10-9/10, 12/10	48	6	37.7, 42	1.1 – 7.0	0	0-0.0115	GPT, S	Global data to match the HYTHIRM
465	LaRC M10 Air	5/09-6/09	60	10	30- 50	0.2– 2.1	-1,0,1	0-0.0175	GPT, S	Global data with scaled fence trips
479	LaRC M10 Air	11/10	32	10	30- 50	0.2 – 2.1	0	0-0.020	GPT, S	Global data with scaled fence trips
6961	LaRC M6 Air	8/10	30	6	40	0.6 – 5.8	0	0-0.0175	GPT, S	Global data with scaled fence trips
462 467 481	LaRC M10 Air	2/09 3/09 9/09	13	10	20	0.5 – 1.9	0	0.039, 0.098	PLIF, TSP, MTV	Surface heating and flow field properties

TC = Thermocouple, GPT = Global Phosphor Thermography, TF = Thin Film, TSP = Temperature Sensitive Paints, PLIF = Planar Laser Induced Fluorescence, MTV = Molecular Tagging Velocimetry, S = Schlieren

Arc Jet Testing

The following is a summary of the arc jet testing that occurred in the JSC Arc Jet Facility. More detailed information about the test article, calibration runs, test procedure, test conditions and results can be found in references 25, 28, 30 and 31. The testing was divided into Phase I (2008) and Phase II (2009) entries. The testing objectives were to determine whether or not the BRI-18 tile protuberance was safe to fly, verify the viability of a BRI-18 trip, provide temperature data on the protuberance tile and localized tile region at representative high enthalpy flight conditions, acquire time-at-temperature slumping performance data on the 0.25-inch flight protuberance at representative flight conditions, perform an arc jet run at conditions that would mimic the flight environment for an oncoming turbulent boundary layer and to enhance understanding of the arc jet testing environment on tile protrusions. As a side objective, it was desired to see what effects the arc-jet flow would have on the temperature indicating paint in order to determine if it could be used for further testing and/or on the flight vehicle.

In Phase I three 0.25-inch and one 0.35-inch protuberance runs were completed in June 2008 using a 10-pack heater. The 0.25-inch protuberance was tested at temperatures from 1200-2000+ deg F while the 0.35-inch protuberance tile was tested at 1900 to 2250+ deg F (detailed test conditions are shown in Table 4). At the highest temperatures the 0.25-inch protuberance tile did show some RCG surface texture changes but no melting or slumping. The phase I test series successfully demonstrated that the 0.25-inch protuberance could survive an arc-jet environment similar to the nominal re-entry environment. No issues (shape change, discoloration, visible damage) with the 0.25-inch protuberance were noted. For the fourth run in the Phase I series, the 0.35-inch protuberance was used and the opposite wall was polished. The protuberance reached the material temperature limit (near 2900 °F) and produced an onset of protuberance shape change. There were clear indications of RCG flow on the protuberance, in the locations where the local temperatures approached 2900 deg F for approximately 60 seconds at the end of the run.

Phase II was initiated because the maximum temperatures during the Phase I barely reached the slumping temperature for the 0.35-inch protuberance. In order to increase the temperatures a 14-pack heater was utilized. Three runs were completed October-December 2009 (between STS-128 and STS-131) with test conditions shown in Table 5. Temperatures on the protuberance reached 3000+ deg F for the last of the three runs and resulted in slumping of the protuberance, shown in Figure 20 and Figure 21, with a maximum height deviation of 0.123 inches from the pre-test OML. As a result of the Phase II testing, it was shown that the protuberance could survive nominal Space Shuttle re-entry conditions. The failure mode for the protuberance was demonstrated and showed that in an overheating condition causing material failure, the protuberance melted until it reached a condition at which the heating was not

enough to cause further melting. This melting caused the downstream temperatures to decrease. The testing was able to demonstrate the first successful use of a 14-pack heater configuration for ARMSEF. Additionally, based on the behavior of the temperature indicating paint in the arc jet testing, the paint was not used for the flight vehicle.

Table 4: Phase I Arc Jet Test Conditions

Target Temperature (°F)		Bulk Enthalpy	Mass Flow Rate	Test Profile 1 0.25" trip	Test Profile 2 0.25" trip	Test Profile 3 0.25" trip	Test Profile 4 0.35" trip
OML	Protuberance	(Btu/lbm)	(lbm/sec)	(sec)	(sec)	(sec)	(sec)
1200 ± 25		> 4000	0.2	100	100	90	-
1500 ± 25		> 5800	0.20 - 0.25	200	200	190	130
1600 ± 25		> 5500	0.25 - 0.30	200	-	-	-
1700 ± 25		> 6000	0.25 - 0.35	200	200	-	-
1800 (optional)		> 6000	0.30 - 0.35	-	200	210	220
2000 (real time)		> 8000	0.30 - 0.35	-	-	210	320
2000 (real time)	2300 (real time)	N/A	0.30 - 0.35	-	-	130	-
	2900 (real time)	N/A	0.35 - 0.40	-	-	-	55

Table 5: Phase II Arc Jet Test Conditions

Run Number	Target Temperature		Calibrated Temperature		Flow Rate	Arc Current	Bulk Enthalpy	Comments
	deg F		deg F		(lbm/sec)	(amps)	(Btu/lbm)	
	OML	Protuberance	OML	Protuberance				
1-3518-9	1200 ± 25	-	1195	-	0.2	500	5336	steady state not achieved
1-3518-9	1500 ± 25	-	1488	-	0.2	1000	7590	
1-3518-9	1700 ± 25	-	1698	-	0.28	1250	7677	
1-3518-9	2000 ± 25	-	1994	-	0.35	1700	8000	
1-3539-9	-	2400 ± 25	1812	2386	0.35	1340	7835	
1-3539-9	-	2600 ± 25	2039	2625	0.4	1850	8573	
1-3539-9	-	2800 ± 25	2096	2792	0.5	1850	8007	
1-3539-9	-	2900 ± 25	2120	2879	0.55	1850	7825	
1-3543-9	-	3100 ± 100	2393	2944	0.55	1850	7870	opposite wall polished



Figure 20: Close up after Run 1-3543-9



Figure 21: Shape Change after Run 1-3543-9

CUBRC Testing

When the opportunity to test in the CUBRC LENS I Facility presented itself, the decision was made to collect data on ten runs at Mach 14 (compared to a maximum of Mach 10 from the NASA LaRC tunnels). The MH-13 model was utilized and additional instrumentation was added to simulate the instrumentation on the flight vehicle. All runs were at 40 deg AoA and 0 deg side slip. While three protuberance heights were manufactured, only the smallest (0.0075-in) and largest (0.0150-in) were tested, with the heights determined using the BLT Tool v.2 correlations and corresponding to flight protuberance heights of 0.42 and 0.83-inches if scaled geometrically. Five runs were completed with each protuberance height in an effort to identify the insipient and fully effective Reynolds numbers. Because no boundary layer trips were used on the centerline, the centerline heating appeared to remain laminar at all conditions tested, as expected. More detailed information about the test article, calibration runs, test procedure, test conditions and results can be found in the preceding sections as well as in references 16, 23 and 24.

One set of thermocouples was along the predicted centerline of the protuberance influenced wedge in order to determine the onset and progress of BLT. Another set of thermocouples was placed across the wedge span to evaluate the spreading angle. From the wedge centerline plot (Figure 22)

) it can be seen that at the lowest Reynolds numbers ($0.73 \times 10^6/\text{ft}$ and $0.16 \times 10^6/\text{ft}$) tested for each protuberance height ($k=0.0075\text{-in}$ and 0.015-in) the flow remained essentially laminar though there may be a very minor influence evident after $x=22.5$ inches. Non-laminar behavior was evident at the next highest Reynolds numbers leading to an incipient BLT Reynolds number for $k=0.0075\text{-inch}$ of between $0.73 \times 10^6/\text{ft}$ and $1.15 \times 10^6/\text{ft}$ and between $0.16 \times 10^6/\text{ft}$ and $0.44 \times 10^6/\text{ft}$ for $k = 0.015\text{-inch}$. The flow appeared to be turbulent by the maximum Reynolds number tested for each of the two heights, making the fully effective BLT Reynolds number for $k=0.0075\text{-inch}$ between $1.78 \times 10^6/\text{ft}$ and $2.14 \times 10^6/\text{ft}$ and between $0.77 \times 10^6/\text{ft}$ and $1.16 \times 10^6/\text{ft}$ for $k = 0.015\text{-inch}$. The axial data across the protuberance wedge is shown in Figure 23 and indicated similar results as the wedge centerline data.

A similar story was evident when looking at the temperature sensitive paint data. While a disturbance appeared evident at all Reynolds numbers tested for both protuberance heights, the transitional/turbulent wedge did not appear to fully develop until the highest Reynolds numbers, with an expanding wedge angle as the Reynolds number was increased. A select set of the images for the 0.0075-inch boundary layer trip is shown in Figure 24.

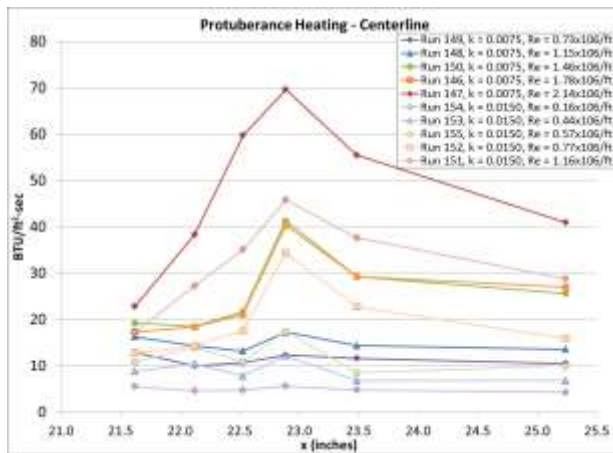


Figure 22: Centerline Heating for $k=0.0075$ and 0.015-inch Protuberances

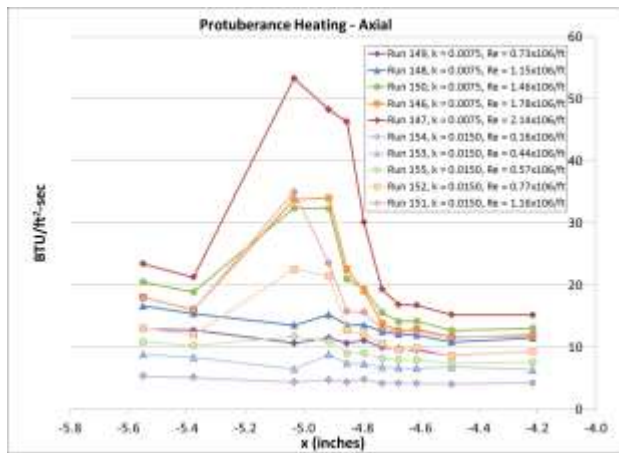


Figure 23: Axial Heating for $k=0.0075$ and 0.015-inch Protuberances

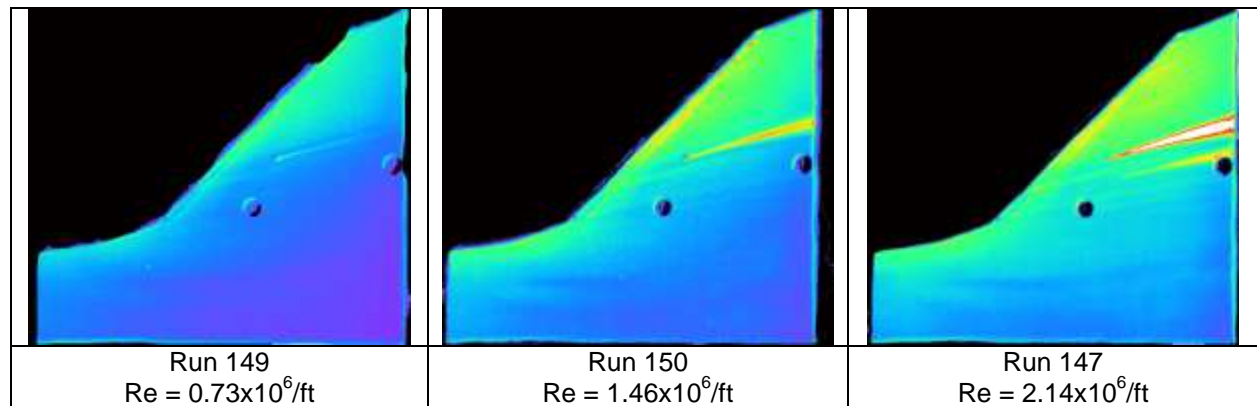


Figure 24: Temperature Sensitive Paint Images of $k=0.0075\text{-Inch}$ runs

Phosphor Thermography Testing

Several separate test entries were made into the NASA LaRC Aerothermodynamics Laboratory facilities using ceramic wind tunnel models and global phosphor thermography. These tests were in support of the BLT DTO FE, FAP and the HYTHIRM programs. The information provided in this section represents an overview of the data collected with respect to the angle of attack, side slip angle, Reynolds

number, Mach number, protuberance height and protuberance shape effects. All phosphor thermography data were normalized using Fay-Riddell stagnation point heating.

a. Angle of Attack and Side Slip Effects

While the majority of the test entries were at the nominal Space Shuttle re-entry angle of attack of 40 deg, runs were completed at other angles of attack from 30-50 degrees.

In the Mach 10 Tunnel for both the centerline and the axial data, as shown in Figure 25, the heating outside of the boundary layer trip's region of influence showed a slight increase as the angle of attack was increased. In the region influenced by the protuberance, the peak heating magnitude did not differ significantly from 40-50 degrees but was slightly lower for the 30-35 degrees.

In the 20-Inch Mach 6 Air Tunnel, only 30-40 degree angles of attack were tested. The centerline had a slight increase in the heating from 30 to 40 degrees. As shown in Figure 26, there were more significant differences when the axial data was considered. At 30 degrees there was a small increase associated with the transitional wedge from the protuberance and from the global heating image it appeared that the flow may not have been turbulent (Figure 27). The peak heating then increased significantly as the angle of attack was increased to 35 and 40 degrees.

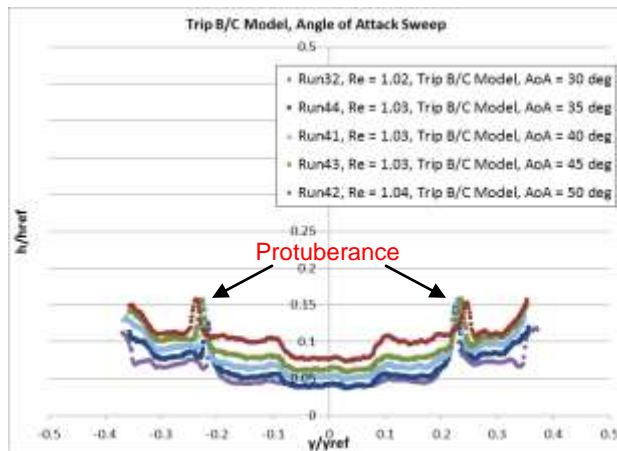


Figure 25: Mach 10, Angle of Attack, Axial

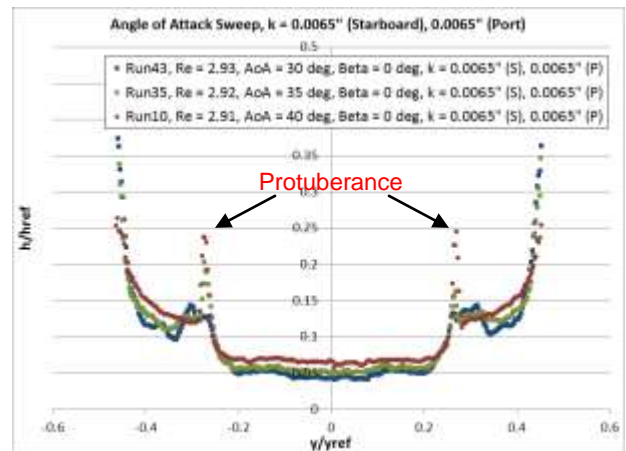


Figure 26: Mach 6, Angle of Attack, Axial

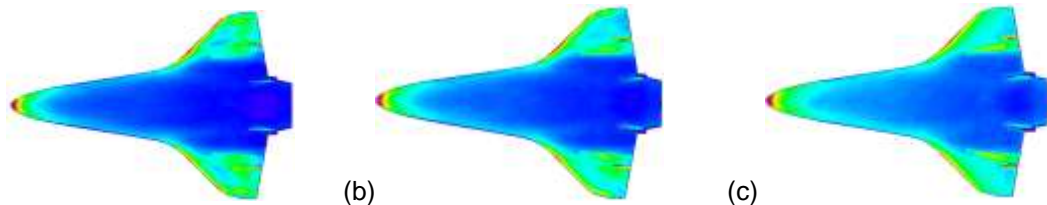


Figure 27: Test 6949, Heating Images at (a) 30 deg AoA, (b) 35 deg AoA, (c) 40 deg AoA

Very few side slip runs were completed, with only a single run at a -1 deg side slip in the Mach 10 Tunnel. There was no significant different on the centerline and axially only a slight offset in the location of the peak but not the magnitudes. In the Mach 6 Air Tunnel side slip angles of 2 and 4 degrees were tested at two Reynolds numbers. The centerline heating data did not show any impact from the side slip angle but the axial data exhibited a definite shift in the heating peak locations as the side slip angle was increased.

b. Reynolds Number Effects

A range of Reynolds numbers were tested in each of the NASA LaRC facilities (0.13-0.31x10⁶/ft in the 20-Inch Mach 6 CF₄ Tunnel, 0.24-2.08x10⁶/ft in the 31-Inch Mach 10 Air Tunnel and 0.59-6.95x10⁶/ft in the 20-Inch Mach 6 Air Tunnel). In the absence of protuberances or natural boundary layer transition, increased Reynolds numbers did not result in significant increased heating on the centerline of the models at any angle of attack tested. As Reynolds number was increased, natural boundary layer transition became evident on the aft ends of the models as well as on the wings. Examples of data from

the Mach 10 and Mach 6 Air Tunnels are shown in Figure 28 and Figure 29. In both cases, the peak heating from the transitional/turbulent wedge associated with the protuberance increased as the Reynolds number was increased. In the Mach 10 case, the lowest Reynolds numbers appeared to be laminar. No cases in the Mach 6 data were laminar but there did appear to be some transitional cases. Both tunnels exhibited increased heating on the wings at higher Reynolds numbers (it was not unusual for one wing to exhibit BLT before the other - one theory was slight roughness differences on the leading edges of the wings leads to differences in the onset of transition).

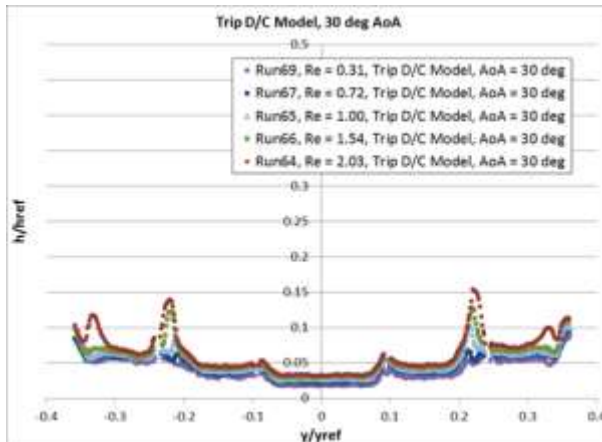


Figure 28: Mach 10, Reynolds Number, Axial

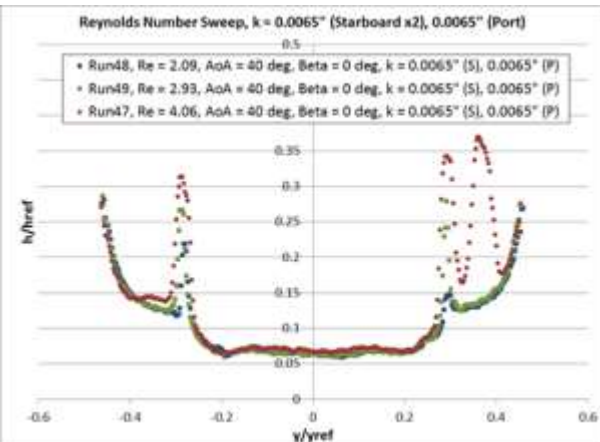


Figure 29: Mach 6, Reynolds Number, Axial

c. Mach Number Effects

The same wind tunnel model configurations were used in the three hypersonic tunnels at NASA LaRC (20-Inch Mach 6 Air, 20-Inch Mach 6 CF₄ and 31-Inch Mach 10 Air). Because of overlapping conditions at the top and bottom of the Reynolds number ranges available in some of the facilities, comparisons could be made with the different Mach numbers and test gases. In general, differences in the tunnels were most evident in the spreading angle of the transitional/turbulent wedges associated with protuberances on the models. When comparing the results from the two air facilities, Figure 30 shows that although the Reynolds numbers between the two runs were relatively close, the turbulent spreading associated with the STS-119 protuberance in Mach 6 was significantly more than in Mach 10, spreading enough to wash over the starboard wing leading edge and onto the port inboard elevon. Comparisons between the Mach 6 CF₄ Tunnel and the other two facilities were little more difficult but a Reynolds number of approximately 0.25×10^6 /ft was run in both the Mach 6 CF₄ Tunnel and the Mach 10 Air Tunnel. The closest comparable Reynolds number in the Mach 6 Air Tunnel was 0.59×10^6 /ft. These three runs are shown in Figure 31 and on the centerline, laminar, heating levels were the same for all three facilities but the wing heating increased for both the air tunnels. An increase in heating due to the protuberance could be seen in both of the Mach 6 sets of data (air and CF₄) but did not appear to be present in the Mach 10 data, supporting a theory that it was harder to produce transitional and turbulent heating in the Mach 10 Tunnel. When comparing the two Mach 6 facilities, the peak heating associated with the protuberance as well as the spreading angle were larger in the air tunnel than in the CF₄ tunnel, where the transitional/turbulent wedge appeared only as a very narrow disturbance.

d. Trip Height and Geometry Effects

Different protuberance designs were tested in the LaRC facilities, including 0.05x0.05 inch kapton tape “pizza box” trips (heights of 0.0035 to 0.0150 inch) and fence trips (heights of 0.006 to 0.0175 inch).

A Mach 6 comparison of the tape trips is shown for the STS-119 model in Figure 32 (chosen as an example because of the range of trip heights tested). The port (negative) side of the model had the BLT DTO protuberance. The smallest protuberance tested was 0.0045 inches and only produced a small heating disturbance. The flow was transitional but not turbulent. All other runs used 0.0065-inch protuberances and were turbulent. Therefore, at Mach 6 Air the insipient transition protuberance height was less than 0.0045 inches and the effective height was between 0.0045 and 0.0065 inches. In Mach 10, the only trip heights tested were 0.0065 inches (resulting in non-turbulent disturbances, thus the insipient trip height was less than 0.0065 inches) and 0.009 inches (resulting in surface temperatures that

exceeded the phosphor thermography range at the peak so heating value could not be determined. Based on comparisons with the starboard side, it appeared that the flow would have been turbulent, resulting in an effective trip height of between 0.0065 and 0.009 inches). On the starboard side of the model (positive), a protuberance was placed to replicate the flight asymmetric boundary layer transition (ABLT). In the Mach 6 Tunnel, protuberances of 0.0035-0.0115 inches were tested. The smallest protuberance, 0.0035-inch, remained laminar and the 0.0065-inch protuberance resulted in turbulent flow. Therefore both the incipient and effective trip heights were between 0.0035 and 0.0065 inches. As the protuberance height was increased to 0.009 and 0.0115-inch, the region of turbulent heating remained the same on the outboard/starboard side but expanded on the inboard/port side. In the Mach 10 Tunnel the smallest protuberance, 0.009 inches, produced a small disturbance and was probably very close to the incipient trip height while both the 0.0115 and 0.0150 protuberances resulted in turbulent heating. The effective trip height was therefore between 0.009 and 0.0115 inches.

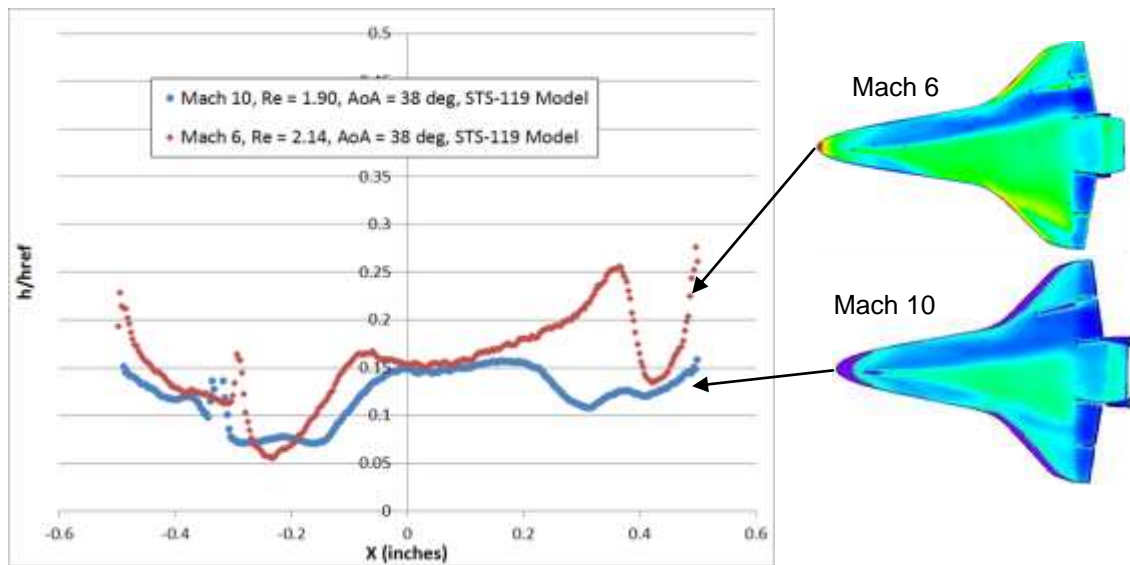


Figure 30: Comparison of Mach 10 and Mach 6 Air on Spreading Angle

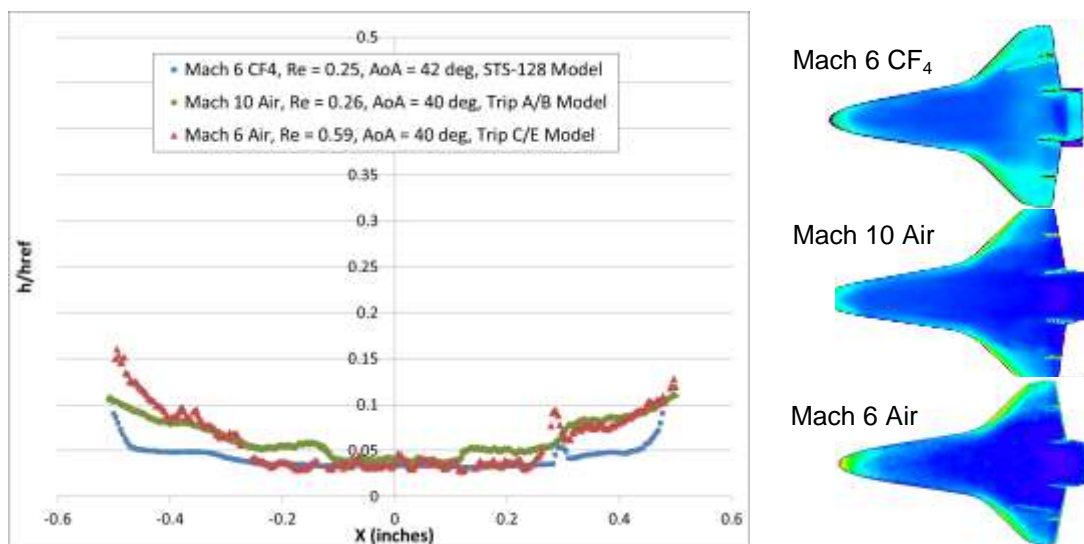


Figure 31: Comparison of Mach 10 Air and Mach 6 Air and CF₄ on Spreading Angle

For the fence protuberances, Figure 33 shows results from the Mach 6 Air Tunnel at a Reynolds number of approximately 2×10^6 /ft. All of the protuberance heights caused BLT and all but the smallest, 0.006-inch, peaked at the same heating rate, with the 0.006-inch peak just slightly below that level. For

Mach 6 Air the incipient trip height was less than 0.006 inches and the effective trip height was between 0.006 and 0.010 inches, though probably closer to the 0.006 inch height. For Mach 10 Tunnel, results are shown in Figure 34. The highest trips tested were 0.0149 and 0.0203-inch with both having the same peak heating rate.

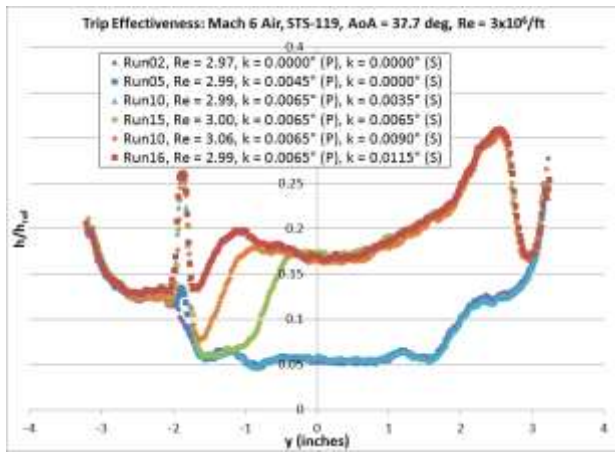


Figure 32: Kapton Trip Effectiveness for STS-119 Configuration in the Mach 6 Air Tunnel

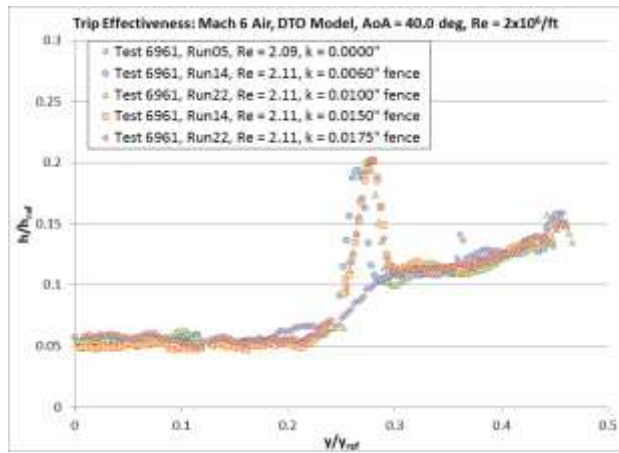


Figure 33: Fence Trip Effectiveness for DTO Configuration in the Mach 6 Air Tunnel

A direct comparison of the kapton and fence trips is shown in Figure 35 for the Mach 6 Air Tunnel. Data are presented in the bump factor format (based on the laminar centerline heating), to eliminate any model-to-model and tunnel-to-tunnel differences as well as allowing for the augmentation due to the protuberances to be determined. The 0.006-inch fence protuberance had a peak bump factor of 3.75 while the 0.0065-inch kapton tape trip data had a peak at about 3.0. When the 0.01-inch and 0.0115-inch protuberances were compared, both had peak bump factors of roughly 3.5. In the Mach 10 Tunnel, when the 0.009-inch kapton tape trip was compared to the 0.0065 and 0.0102-inch fence protuberances, the kapton trip heating had a peak bump factor of 1.8 as compared to 2.4-2.6 for the fence trips. The bump factors for the fence trips were in line with values in previous testing³² but the kapton bump factors were well below, indicating that the flow may not have been turbulent.

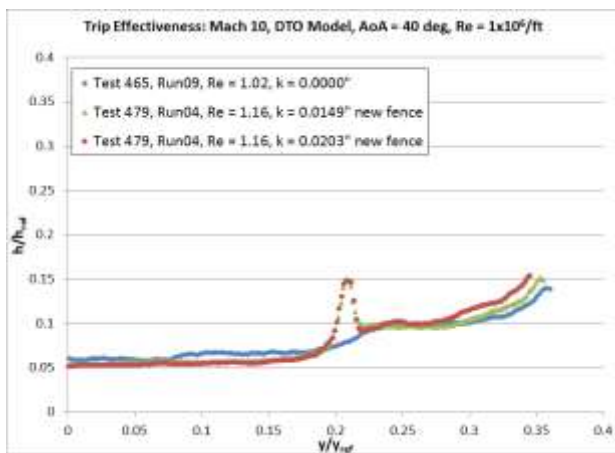


Figure 34: New Fence Trip Effectiveness for DTO Configuration in the Mach 10 Air Tunnel

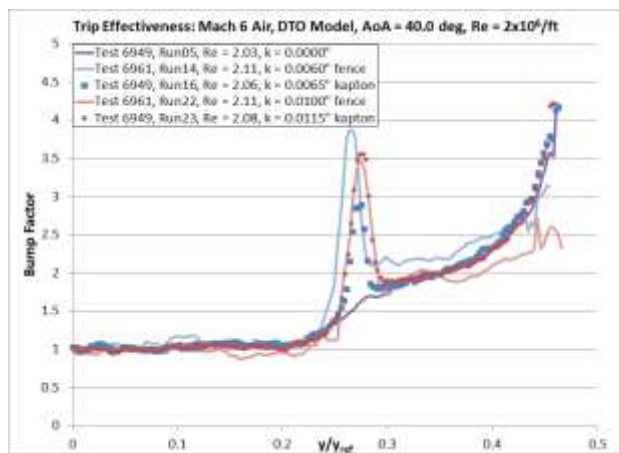


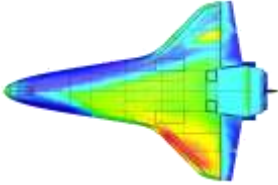
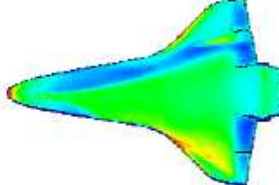
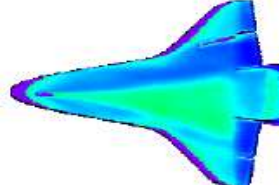
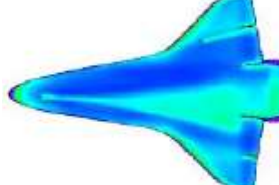
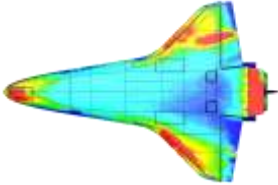
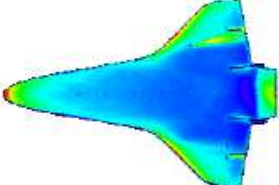
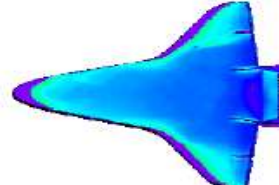
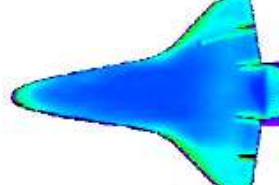
Figure 35: Kapton vs. Fence Trip Effectiveness in the Mach 6 Air Tunnel

e. Mission Specific Effects

A series of the phosphor thermography tests were completed in direct support of the HYTHIRM flight data collections during BLT FE flight on STS-119 and STS-128 (both flown on OV-103, *Discovery*) as well as the non-BLT FE flights on STS-125 and STS-132 (both flown on OV-104, *Atlantis*, and not discussed in this report). The models used for this test series had body flap and elevon configurations that

represented the flight control surface deflections at the time of closest approach for the HYTHIRM observation and were tested at the flight specific angles of attack. The other BLT FE missions had not flown at the time of model construction. The models were tested in the 20-Inch Mach 6 Air, 31-Inch Mach 10 Air and 20-Inch Mach 6 CF₄ Tunnels. The STS-119 flight image, captured at approximately Mach 8.5, showed the BLT FE-related wedge on the port wing as well as a large ABLT on the starboard side of the vehicle, extending from approximately the nose landing gear location and washing the majority of the starboard side of the vehicle in turbulent flow as early as Mach 11.5. The cause was never positively identified but may have been as small as 0.1-inch, well within the step-and-gap criteria for the flight vehicle and not a safety-of-flight issue. The STS-128 image was captured at approximately Mach 15 and showed the BLT FE-related wedge on the port wing but the remainder of the vehicle laminar at that Mach number. For comparison to each of these flights, boundary layer trips of various heights were placed on the wind tunnel models in the approximate locations of the flight protuberances. Models were tested through a variety of Reynolds numbers to determine the effects. Side by side comparison of the flight data and the most representative image from each tunnel are shown in Table 6 (scales differ). The ground test data was able to qualitatively match well with the flight data in terms of spreading angle and acreage affected by protuberances. The best comparisons were between the Mach 6 Air Tunnel and flight. This data can be used to improve the ground-to-flight extrapolation techniques and compliments the other data sources including computational (not shown) data.

Table 6: Comparison of Flight and Ground Test Heating Patterns

Flight	20-Inch Mach 6 Air	31-Inch Mach 10 Air	20-Inch Mach 6 CF ₄
			
STS-119 BLT FE Flight Mach 8.4	Test 6963, Run 17 Re = 3.06×10^6 /ft k = 0.009" (fwd), 0.0065" (wing)	Test 475, Run 03 Re = 1.90×10^6 /ft k = 0.015" (fwd), 0.009" (wing)	Test 170, Run 04 Re = 0.308×10^6 /ft k = 0.015" (fwd), 0.009" (wing)
			
STS-128 BLT FE Flight Mach 14.7	Test 6963, Run 24 Re = 2.97×10^6 /ft k = 0.0065" (wing)	Test 475, Run 13 Re = 1.93×10^6 /ft k = 0.009" (wing)	Test 170, Run 10 Re = 0.252×10^6 /ft k = 0.009" (wing)

Smaller trips were required in the Mach 6 Air Tunnel than in the other tunnels in order to re-create the flight heating patterns and identical trip heights were used in the other two tunnels, Mach 6 CF₄ and Mach 10 Air. The spreading angle of the turbulent wedge was greater in the Mach 6 Air Tunnel, followed next by the Mach 10 Air Tunnel and smallest in the Mach 6 CF₄ Tunnel (Figure 36), a trend observed at NASA LaRC and other facilities.^{33, 34} The maximum Reynolds numbers for the Mach 10 and Mach 6 CF₄ Tunnels were utilized and in some cases, especially CF₄, were not enough to recreate flight observed conditions.

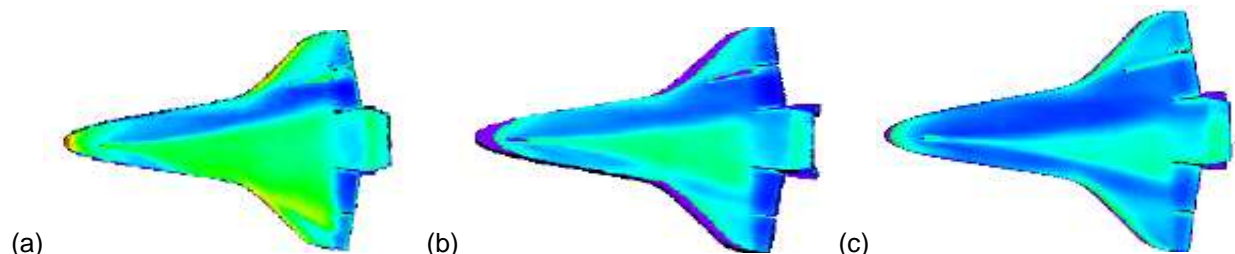


Figure 36: (a) Mach 6 Air, Reynolds Number = 2.14×10^6 /ft, (b) Mach 10 Air, Reynolds Number = 1.9×10^6 /ft, (c) Mach 6 CF₄, Reynolds Number = 0.31×10^6 /ft

PLIF and TSP Testing

The following is a summary of the PLIF and TSP testing that occurred in the LaRC 31-Inch Mach 10 Air Tunnel. More detailed information about the test article, calibration runs, test procedure, test conditions and results can be found in the preceding sections as well as in references 16 and 21. The testing was divided into three tunnel entries between 2009 and 2011 in support of the BLT FE and part of a larger ground test program to demonstrate PLIF and TSP capabilities. These tests examined the flow field surrounding and downstream of the protuberance as well as the surface heating effects. This testing differed from the global phosphor thermography testing in that local conditions in the immediate vicinity of the protuberance were examined as opposed to global effects.

For the PLIF runs, the height of the laser sheet was varied and an example image of the PLIF results is shown in Figure 37. Because the protuberance blocked the laser directly below itself, a shadow appears in many of the images. The protuberance pushed the flow to the side (above in the image) of the protuberance and instability streaks were present directly downstream of the protuberance. At some distance downstream, these instability streaks transitioned to turbulent flow in most cases. At lower Reynolds numbers, little change was seen with laminar flow leading up to the protuberance and some streamwise streaks were present downstream of the protuberance but no turbulence. This was true both at the model surface and away from the surface. Streaks were still present at 0.059 inches above the model (with a 0.039-inch protuberance). As the Reynolds number was increased the streaks seemed to show more evidence of instability away from the surface. This seemed to support the theory that boundary layer transition in hypersonic flow begins at the edge of the boundary layer and propagates down to the surface. At the highest Reynolds number tested it appeared that the flow downstream of the protuberance was turbulent.

For the TSP the center insert contained the protuberance and the two outer inserts were flat “blanks” (shown in Figure 38). Increased heating was noted on the center insert with a very strong streak below the protuberance and a weaker one above the protuberance. There was also a small region of increased heating immediately in front of the protuberance. Lower than baseline heating was noted further upstream of the protuberance as well as directly downstream of the protuberance, between and outboard of the streaks. As the Reynolds number was increased, the streaks increased in intensity and size.

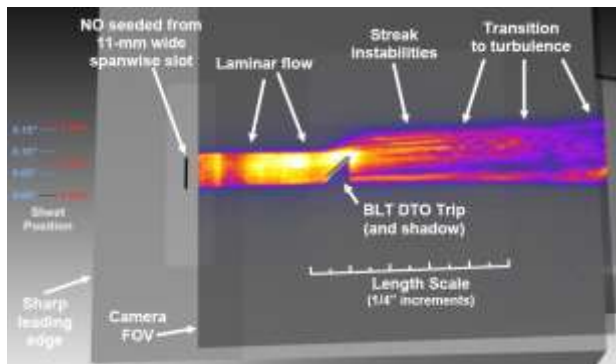


Figure 37: ViDI rendering of NO PLIF image

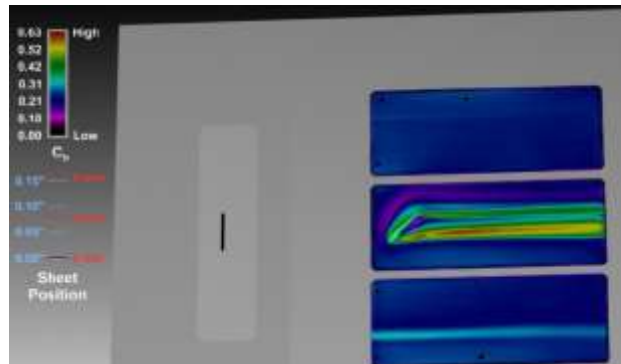


Figure 38: ViDI rendering of TSP image

As an interesting comparison, because of the degradation to the TSP inserts (made of NanoForm), a qualitative comparison could be made between the arc jet test articles and the TSP test articles, shown in Figure 39. The resulting flow patterns appeared to be very similar with strong indications of heating coming off of both corners of the protuberances.

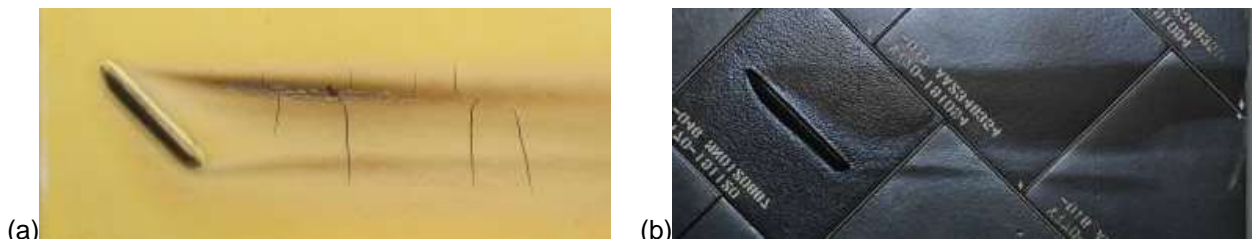


Figure 39: Heating Patterns in (a) LaRC Mach 10 - TSP, (b) JSC arc jet - Shuttle Tile

Two runs were completed using laser velocimetry, one with a 0.039-in protuberance and one with a 0.098-in protuberance. Both runs were at a Reynolds number of $0.5 \times 10^6/\text{ft}$. Figure 40 shows the velocity profile for the 0.098-inch protuberance. The trip is represented by the gray boundary. The four plots show profiles at 0.031, 0.043, 0.091 and 0.134 inches above plate. For the profile closest to the plate, the flow on the windward side of the protuberance was deflected slightly away from the protuberance. The view on the leeward side of the protuberance was blocked because the protuberance blocked the laser sheet. Downstream of the protuberance, the flow began to accelerate and the profiles for all downstream locations exhibited curvature, especially directly downstream of each edge of the protuberance. Profiles slightly further from the surface showed the same general trends with increased velocities. When the laser sheet was 0.091-inch above the plate, the sheet was nearly passing over the protuberance. The velocities on the leeward side of the protuberance were significantly higher than those on the windward side of the protuberance. Downstream of the protuberance, the only effect noted in the velocity profiles was the curvature at the trailing edge corner which increased in magnitude as the distance downstream was increased. By the time the laser sheet was at 0.134-inches above the plate, well above the protuberance, there appeared to be some impact to the velocity profiles above the protuberance, but little or no influence downstream. Further results are shown in reference 22.

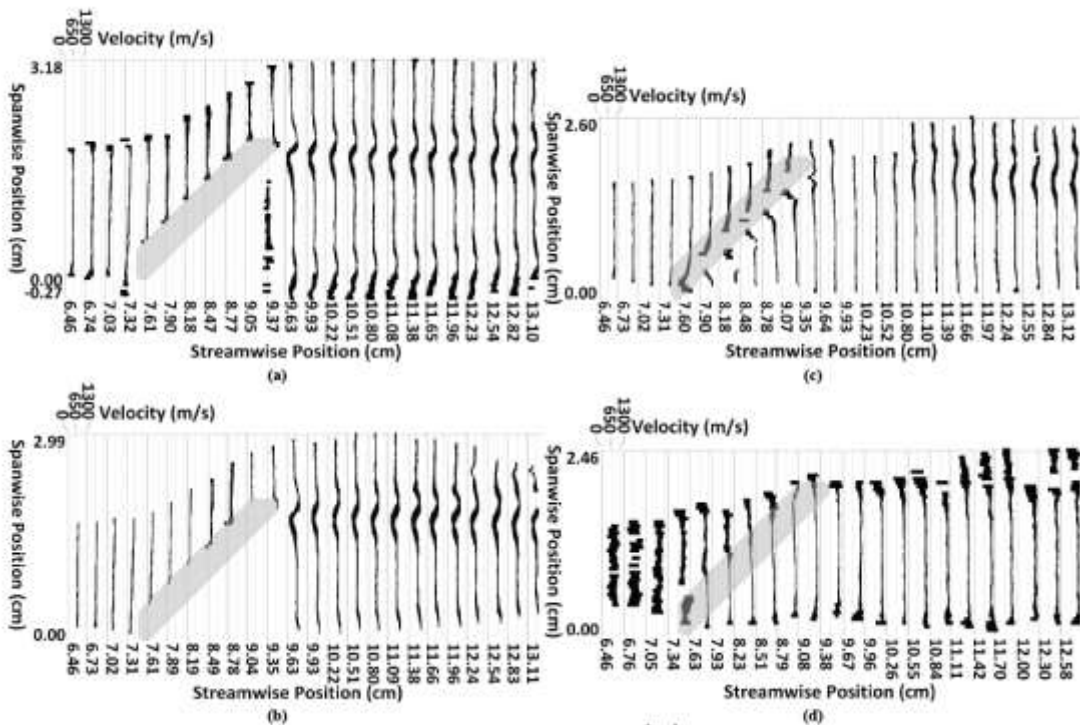


Figure 40: 0.098-in Protuberance Velocity Profiles (a) 0.031 (b) 0.043 (c) 0.091 (d) 0.134-in above plate

Conclusions

In support of the Space Shuttle BLT FE, a series of ground tests were completed at NASA JSC, NASA LaRC and CUBRC. The tests supported pre-flight certification and safety requirements as well as provided a set of discrete and global data for comparison to the predictions and flight data (both discrete and global) and for use in improving predictions methods and ground-to-flight correlations.

During the arc jet testing in the NASA JSC ARMSEF, both 0.25 and 0.35-inch protuberances were tested and flight-like temperatures were demonstrated on the protuberances and surrounding tiles. Surface and bondline temperatures were monitored and all bondline temperatures stayed within the material safety limits. The 0.35-inch protuberance was taken to 2900 deg F, the material limit, and exhibited minor shape change with some of the RCG coating melting. When tested at 3100 deg F, the protuberance exhibited a major failure, yielding important information on the nature of the material failure.

These tests showed that the protuberance would be safe for flight and that in the event of a failure, the protuberance would slump until it was small enough that the heating would not yield further melting.

Testing in the CUBRC facility collected Mach 14 data over a range of Reynolds numbers. Flight scaled protuberances were tested and the insipient and effective Reynolds numbers for each protuberance height were determined. Global TSP data was taken for comparison to the flight data.

Seven global phosphor thermography test entries were completed in the NASA LaRC hypersonic wind tunnels (20-Inch Mach 6 Air, 31-Inch Mach 10 Air and 20-Inch Mach 6 CF₄ Tunnels). These tests were in support of flight experiment planning (one test), HYTHIRM (three tests) and FAP (three tests). In general, as the angle of attack of the model was increased, the heating rates increased. Changes to the side slip angle did not significantly affect the magnitudes of the heating associated with the protuberances but did shift the peak location. Higher Reynolds numbers led to natural BLT on the wing and aft fuselage sections of the models, especially in the Mach 6 Air Facility. Increased Reynolds number also led to increased peak heating associated with the protuberance wedge. When similar Reynolds numbers were compared between the various facilities, it was shown that the spreading angles associated with the 20-Inch Mach 6 Air Tunnel were the largest. It proved more difficult to produce turbulent conditions in the Mach 10 Air and Mach 6 CF₄ Tunnels and both routinely exhibited smaller spreading angles. Boundary layer trip effectiveness was compared (kapton tape/square trips versus metal/fence trips) in the various LaRC tunnels. Insipient and effective protuberance heights were determined based on data collected in the Mach 6 and Mach 10 Air Tunnels at various locations, including the BLT FE protuberance location and a trip associated with the STS-119 ABLT. The larger the protuberance, the more effective it was at producing transitional or turbulent flow. Testing in the LaRC tunnels was used to recreate data collections made by the HYTHIRM team on STS-119 and 128. The models for these tests differed from the other LaRC tests because they incorporated control surface deflections that matched the HYTHIRM observations and were tested at flight specific angles of attack. Data yielded global images which were available for comparison to the flight global images collected.

PLIF and TSP testing was also completed in the NASA LaRC 31-Inch Mach 10 Air Tunnel. Various protuberance configurations were tested and by varying the laser sheet location, the behavior of the flow off the surface of the model and downstream of the protuberance was imaged using PLIF. TSP images were taken and compared qualitatively to the PLIF data to understand the heating on the surface of the model. MTV was used on a small number of runs to determine the flow velocities at various locations at and downstream of the protuberance.

With the completion of the ground testing, the hope is that the data collected will be valuable as part of a larger set of data for the flight program, including computation predictions, ground test data (discrete and global) and flight data (discrete and global). Although the Space Shuttle is not flying anymore, the data collected as a part of this program may still prove valuable in the advancement of both computation prediction strategies and ground-to-flight extrapolation for future programs.

References

1. Campbell, C.H., Anderson, B.P., King, R.A., Kegerise, M.A., Berry, S.A., Horvath, T.J., "Roles of Engineering Correlations in Hypersonic Entry Boundary Layer Transition Prediction", AIAA 2010-247, January 2010.
2. Berry, S.A., Bouslog, S.A., Brauckmann, G.J., Caram, J.M., "Shuttle Orbiter Experimental Boundary-Layer Transition Results with Isolated Roughness", Journal of Spacecraft and Rockets, 1998, Vol. 35, No.3, (241-248).
3. Berry, S.A., Horvath, T.J., Greene, F., Kinder, G.R., Wang, K.C., "Overview of Boundary Layer Transition Research in Support of Orbiter Return to Flight", AIAA 2006-2918, June 2006.
4. Berry, S., A., Hamilton, H., "Discrete Roughness Effects on Shuttle Orbiter at Mach 6", AIAA 2002-2744, June 2002.
5. Anderson, B. P., Campbell, C. H., Saucedo, L. A., Kinder, G. R., Berger, K. T., "Boundary Layer Transition Flight Experiment Overview and In-Situ Measurements," AIAA 2010-0240, January 2010.
6. Berger, K., Anderson, B., Campbell, C., Garske, M., Saucedo, L., Kinder, G., Micklos, A., "Boundary Layer Transition Flight Experiment Overview," AIAA-2011-3323, June 2011
7. Horvath, T.J., Tomek, D.M., Berger, K.A., Zalameda, J.N., Splinter, S.C., Krassa, P.W., Schwartz, R.J., Gibson, D.M., Tietjen, A.B., Tack, S., "The HYTHIRM Project: Flight Thermography of the Space Shuttle during Hypersonic Flight", AIAA 2010-241, January 2010.

8. Campbell, C.H., Garske, M.T., Kinder, G., Berry, S.A., "Orbiter Entry Boundary Layer Flight Testing", AIAA 2008-635, January 2008.
9. Berry, S.A., King, R.A., Kegerise, M.A., Wood, W., McGinley, C., Berger, K., Anderson, B.P., "Updates to Orbiter Boundary Layer Transition Prediction Tool," AIAA 2010-246, January 2010.
10. Campbell, C. H., Anderson, B. P., Bourland, G., Bouslog, S. A., Cassady, A., Horvath, T. J., Berry, S. A., Gnoffo, P., Wood, W. A., Reuther, J., Driver, D., Chao, D., "Orbiter Return to Flight Entry Aeroheating", AIAA 2006-2917, June 2006.
11. Hyatt, A.J., Wang, K.C., Everhart, J.L., Green, F., Merski, N.R., Wood, W.A., Berger, K., Anderson, B.P., Cassady, A., "The Cavity Heating Tool: Version 3.0 Documentation", Boeing Technical Memorandum, ATA-AH-TM-2006-035.
12. Berry, S.A., Horvath, T.J., Cassady, A.M., Kirk, B.S., Wang, K.C., Hyatt, A.J., "Boundary Layer Transition Results from STS-114", AIAA 2006-2922, June 2006.
13. Bertin, J.J., Schneider, S.P., Campbell, C.H., "A Flight-Testing Proposal on Roughness-Induced Boundary-Layer Transition on the Space Shuttle Orbiter", NASA White Paper, November 14, 2006.
14. Spanos, T., Kinder, G., Campbell, C.H., Andress, J., "Boundary Layer Transition Flight Experiment Thermal Protection System and Instrumentation Modifications", AIAA 2010-242, January 2010.
15. Rochelle, W.C., Battley, H.H., Grimaud, J.E., Tillian, D.J., Murray, L.P., Lueke, W.J., and Heaton, T.M., "Orbiter TPS Development and Certification Testing at the NASA/JSC 10 MW Atmospheric Reentry Materials and Structures Evaluation Facility", AIAA-83-0147, Reno, NV, January 1983.
16. CUBRC Aerosciences Group Research Staff, "LENS Brochure", Capabilities and Technologies, Buffalo, NY, 2007.
17. Micol J. R., "Langley Aerothermodynamics Facilities Complex: Enhancements and Testing Capabilities," AIAA Paper 98-0147, January 1998.
18. Buck, G. M., "Automated Thermal Mapping Techniques Using Chromatic Image Analysis," NASA TM 101554, April 1989.
19. Merski, N. R., "Reduction and Analysis of Phosphor Thermography Data with IHEAT Software Package," AIAA-98-0712, January 1998.
20. Merski, N. R., "Global Aeroheating Wind-Tunnel Measurements Using Improved Two-Color Phosphor Thermography Model," Journal of Spacecraft and Rockets, Vol., 36, No., 2, 1998, pp. 160-170.
21. Bathel, B., Danehy, P., Inman, J., Watkins, A., Jones, S., Lipford, W., Goodman, K., Ivey, C., Goynes, C., "Hypersonic Laminar Boundary Layer Velocimetry with Discrete Roughness on a Flat Plate," AIAA-2010-4998, June 2010.
22. Bathel, B., Danehy, P., Inman, J., Jones, S., Ivey, C., Goynes, C., "Multiple Velocity Profile Measurements in Hypersonic Flows Using Sequentially-Images Fluorescence Tagging," AIAA-2010-1404, January 2010.
23. Wadhams, T., Holden, M., MacLean, M., Campbell, C., "Experimental Studies of Space Shuttle Orbiter Boundary Layer Transition at Mach Numbers from 10 to 18," AIAA-2010-1576, January 2010.
24. Wadhams, T., Holden, M., MacLean, M., Campbell, C., Anderson, B., Berger, K., Rufer, S., Berry, S., "Experimental Studies of Space Shuttle Orbiter Boundary Layer Transition with Flight Representative Protuberances," AIAA-2011-3328, June 2011.
25. Larin, M., Bulot, E., "Boundary Layer Transition Trip HRSI TPS Tests at NASA JSC Arc-Jet Facility," JSC-64650, September 2009.
26. Danehy, P., Ivey, C., Bathel, B., Inman, J., Jones, S., Watkins, A., Goodman, K., McCrea, A., Lighty, B., Lipford, W., Jiang, N., Webster, M., Lempert, W., Miller, J., Meyer, T., "Orbiter BLT Flight Experiment wind tunnel simulations: nearfield flowfield imaging and surface thermography," AIAA-2010-1571, January 2010.
27. Hubner, J. P., Carroll, B. F., Schanze, "Heat Transfer Measurements in Hypersonic Flow Using Luminescent Coating Techniques," AIAA Journal, Vol. 210, No. 4, 2002, pp. 516-522.
28. Larin, M.E., Marichalar, J.J., Kinder, G.R., Campbell, C.H., Riccio, J.R., Nguyen, T.Q., Del Papa, S.V., Pulsonetti, M.V., "Boundary Layer Transition Protuberance Tests at NASA JSC Arc-Jet Facility", AIAA-2010-1578, January 2010.
29. Everhart, J., "Transition Induced by Fence Geometries on Shuttle Orbiter at Mach 10," AIAA-2010-1577, January 2010.
30. Buck, G.M., Powers, M. A., Griffith, M. S., Hopkins, J. S., Veneris, P. H., Kuykendoll, K. A., "Fabrication of 0.0075-Scale Orbiter Phosphor Thermography Test Models for Shuttle RTF Aeroheating Studies," NASA TM 2006-214507.

31. Larin, M., "Boundary Layer Transition Protuberance Failure Mode Tests at NASA JSC Arc-Jet Facility," JSC-65946, September 2010.
32. Berger, K. T., "Aerothermodynamic Testing of the Crew Exploration Vehicle at Mach 6 and Mach 10," *AIAA Journal of Spacecraft and Rockets*, Volume 46, Number 4, pp. 758-765.
33. Fischer, M.C., "Spreading of a Turbulent Disturbance," *AIAA Journal*, Volume 10, Number 7, pp.957-959.
34. Krishnan, L., Sandham, N. D., "Effect of Mach number on the structure of turbulent spots," *Journal of Fluid Mechanics*, 2006, Volume 566, pp. 225-234.